Direct Simulation Monte Carlo Method in Industrial Applications

Gennaro ZUPPARDI and Francesco ROMANO

Direct Simulation Monte Carlo Method in Industrial Applications

Gennaro Zuppardi and Francesco Romano

Department of Aerospace Engineering - University of Naples "Federico II"
Piazzale Tecchio, 80 – 80125 Naples, Italy

Abstract. In the present work three different applications of DSMC method to problems of industrial interest are revised and deepen by using both other methodologies and a more updated or advanced DSMC code, compared with those already used by other researchers to solve the same problems. For each problem, a preliminary rarefaction analysis verifies that the molecular approach, therefore the use of a DSMC code, is proper. More specifically, in this work the "sophisticated" DS2V (Ver.4.5) code has been used for the simulation of the flow fields in a deposition chamber and in a micro-channel as well as for the evaluation of viscosity of mixtures. The present work is an improvement of former works about the same topics because: 1) a method is proposed for the evaluation of the film distribution on the substrate. Furthermore, as the thin film deposition process is based on expanding thermal plasma from a torch, the influences of mass flow rate and of electrical power, supplied to the gas, and of the fluid-dynamic characteristics of the plasma jet, linked to geometry of different nozzles, are analyzed. 2) Some fluid-dynamic parameters in a micro-channel, such as load loss and impulse have been evaluated. 3) Computation of the exponent of the temperature viscosity law of a mixture of gases is proposed.

INTRODUCTION

A design process relies on a preliminary computer simulation of the project. This simulation is necessary to save money and time. When the project is related to a fluid-dynamic problem in continuum, the numerical simulation is based on "classical" CFD (Computational Fluid Dynamics) approach, namely on the solution of the Navier-Stokes equations. The same methodology is used also for the evaluation of the aerodynamic forces on a spacecraft during the re-entry at high altitude. In this case, due to rarefaction, the "classical" Navier-Stokes equations fail, because of the failure of the transport equations of Newton, Fourier and Fick. It is well known that, nowadays, the Direct Simulation Monte Carlo (DSMC) [1] is the unique method for reliable solution of a rarefied flow field.

Besides space applications, the solution of a rarefied flow field and therefore the use of DSMC is of interest also in some current industrial applications. On the other hands, the research on Rarefied Gas Dynamics (RGD), for industrial applications, already started at the beginning of the 20th century (1910) thanks to the study of low speed, micro-scale flows by Knudsen, Weber and other researchers [2]. For example, Knudsen obtained that the mass flow rate in a pipe gets a minimum in transitional regime (Knudsen paradox). Weber measured the drag of micro-spheres in air. Towards the end of the 20th century (1980), RGD started to consider also the flow fields in Micro-Electron-Mechanical Systems (MEMS). These are very complicated systems because their dimensions are of the order of microns. Currently, other RGD problems in industrial processes are: i) the analysis of the flow field in the region between the read/write head and the hard disk of a computer. In fact, even though air is at ambient conditions, the distance between these two elements is of the order of 50 nm, ii) the prediction of growth and of uniformity of thin films on a surface by deposition and cluster of gas molecules. In fact, a deposition chamber works in rarefied conditions being the pressure of the order of 10 Pa.

The aim of this work is to apply the DSMC method to three different typologies of problems, already considered by other researchers. These problems will be revised and deepen by: i) adding information, ii) using more accurate approaches and iii) running a more updated and advanced or "sophisticated" DSMC code. More specifically, the topics of the present analysis are:

1. simulation of thin film deposition process, already considered by van den Sanden [3, 4] and by Selezneva [5]. In the present work the flow field in a deposition chamber is simulated and a method is proposed for a preliminary evaluation of the film thickness distribution on a surface. Furthermore, as the deposition process is based on expanding thermal plasma from a torch, the influences of mass flow rate, electrical power, supplied to the gas and of the fluid-dynamic characteristics of the plasma jet, linked to different nozzles, are analyzed.
2. Computation of fluid-dynamic parameters in micro-channels, already considered by Le [6], Arkilic [7] and Ho [8]. Le investigated some aerodynamic parameters in a 2D-plane micro-channel in supersonic, transitional regime. In the present work, some important parameters, not yet considered, such as load loss and impulse are evaluated. Knowledge of these parameters is important for a correct design of a pressure micro-transducer.
3. Evaluation of viscosity coefficient, already considered by Bird [1]. In the present work, a method is proposed for the evaluation of the exponent of the dependence law of viscosity on temperature for a mixture of gases. This method relies on the phenomenological definition of shear stress (equations of Newton) and on the evaluation of the velocity gradient at the wall. The method has been implemented considering the flow field on a flat plate.

In order to verify the rarefaction level and therefore the adequacy of using the DSMC method, a preliminary rarefaction analysis is provided for each application.

RAREFACTION PARAMETERS

Three formulations of the local Knudsen number have been considered: $Kn_L=\lambda/L$, $Kn_{LG}=\lambda/L_G$, and $Kn_\delta=\lambda/\delta$ (the latter is called also Tsien parameter), where: λ is the local mean free path, L is a geometrical dimension of the body and L_G is the scale factor of the gradient of a generic macroscopic quantity G:

$$L_G = \frac{G}{(dG/ds)} \tag{1}$$

s is an abscissa in the flow direction, and δ is the local boundary layer thickness. In the case of a flat plate:

$$\delta \cong \frac{x}{\sqrt{Re_x}} \tag{2}$$

The mean free path can be computed by the Stokes law, linking viscosity to the mean free path ($\mu = 0.5\rho\bar{c}\lambda$):

$$\lambda = 1.25\sqrt{\gamma}\frac{\nu}{a} \tag{3}$$

where ν is the kinematic viscosity and a is the sound speed. Therefore Kn_δ reads:

$$Kn_\delta = \frac{\lambda}{\delta} = 1.25\sqrt{\gamma}\frac{M}{\sqrt{Re_x}} \tag{4}$$

According to Bird [1], the classification of a flow field rarefaction, in terms of local Knudsen number, is:

$Kn_{LG}<0.1$	Continuum with validity of the Navier-Stokes equations,
$0.1<Kn_{LG}<0.2$	Continuum without validity of the Navier-Stokes equations (continuum low density),
$Kn_{LG}>0.2$	Non continuum; a molecular approach is necessary.

In the present work, the same criteria have been considered valid also for Kn_L and Kn_δ.

DS2V CODE AND RUN CONDITIONS

DS2V (Ver.4.5) by Bird [9] is a very advanced DSMC code. This code is widely tested and worldwide accepted. DS2V simulates 2-D plane/axi-symmetric flow fields. All procedures, making a DSMC code "sophisticated" [10, 11], are implemented: i) it relies on two sets of cells (collision and sampling cells) with the related cell adaptation, ii) it implements procedures promoting nearest neighbor collisions, iii) it generates automatically computational parameters such as numbers of cells and of simulated molecules by the input number of megabytes, iv) it uses a radial weighting factor in solving axial-symmetric flow fields, v) it provides optimal time step.

All versions of DS2V rely on the same theoretical approach. The differences between the former versions, as per 3.6 and 4.x, x=1,2,3,4, are only technological. Some procedures like input, graphical visualization, cell adaptation and so on are improved. Input has been made easier, with respect to the previous versions. A run can be checked on line by three displays, each one related respectively, to:

1. run parameters, such as simulation time, maximum and averaged value of the ratio of the mean collision separation (mcs) to λ, number of simulated molecules, number of collisions and so on. This display includes also a plot showing the time history of the number of molecules; fluctuations are indicative of a stabilization of the run.
2. 2-D plots of flow field parameters as per velocity, density, pressure, mcs/λ, gas composition and so on.
3. Plots of surface parameters: heat flux, slip velocity, pressure and so on, as functions of curvilinear abscissa.

For all computations, the input number of megabytes was about 120, providing a proper number of cells and of simulated molecules. The numbers of simulated molecules were about 3×10^6, 10^6 and 1.5×10^6 for the three applications, respectively; the condition mcs/λ<1 was met in every runs. Furthermore the simulation time satisfied the condition for a stationary state. This was considered attained when the ratio of simulated time to reference time was between 6 and 10. The reference time is the time necessary to cross the computational domain along the free stream direction.

THIN FILM DEPOSITION

The thin film deposition process (or coating) on a surface, i.e. a substrate, consists in creating a solid layer from chemical reactions in the gas or directly from chemical reactions with the substrate material. A thin film has typically a thickness from 10^{-3} to 10^{2} μm. This technology is of interest in the field of electronic manufacturing such as: magnetic recording media, semiconductors, Liquid Crystal Displays (LCD), solar cells, corrosion protective coating and so on.

Deposition involves purely physical processes such as high temperature vacuum evaporation or plasma sputter bombardment and consists in the growth of a layer by the deposition or aggregation of an atom at a time, impinging onto the substrate. The deposition techniques basically fall into two wide categories, depending on whether the process is chemical (Chemical Vapor Deposition: CVD) or physical (Physical Vapor Deposition: PVD):

1. In the CVD technique, a fluid precursor undergoes a chemical change at the substrate, forming a solid layer.
2. In the PVD technique the deposition is obtained by the condensation of vaporized material onto the substrate.

A type of CVD technique was developed by van de Sanden and co-workers [3, 4] at the University of Eindhowen. This technique considers the deposition of a thin, amorphous film of C:H or of Si:H on the substrate, using the Expanding Thermal arc Plasma method. Figure 1 shows the van de Sanden deposition apparatus, made up of: a torch, a supersonic nozzle, an expansion cylindrical chamber or reactor (diameter 0.16 m, length 0.8 m) and a substrate holder (length 0.35 m, diameter 0.1 m). The diameter of the nozzle exit section or diameter of the chamber inlet section is 0.032 m.

The technique consists in generating thermal plasma of argon or of a mixture of argon and hydrogen at a pressure of 10^{4}-6×10^{4} Pa. Precursor gas species (S_iH_4, C_2H_2 or CH_4) are injected into the nozzle or directly into the reactor, where pressure of 10-10^{2} Pa is hold by a pump. These species react with electrons and ions in the plasma and form radical, reactive species. The plasma mixture expands supersonically into the reactor and then is compressed by a shock wave. The plasma flows toward the substrate where deposition occurs, forming a film.

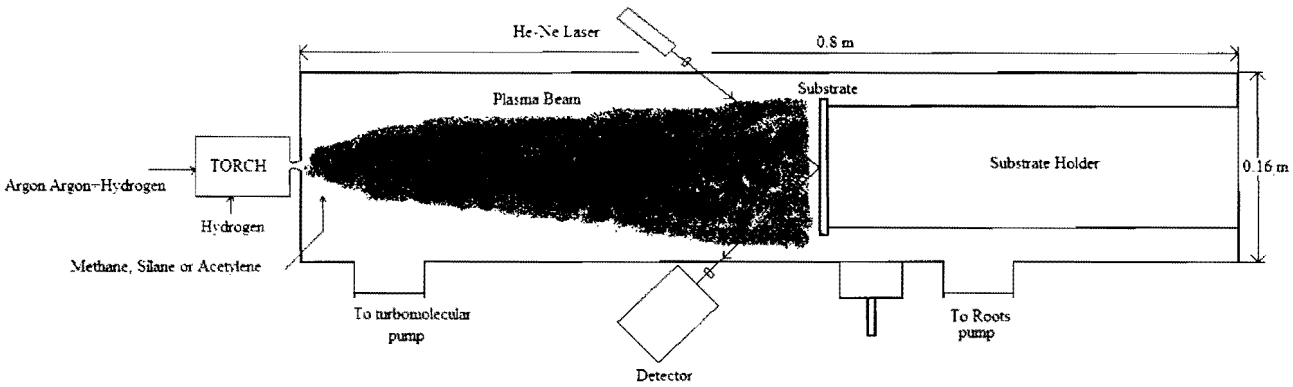

Fig. 1 – van de Sanden deposition apparatus

The present computations simulate the flow field in the system made up of: torch, nozzle and chamber. The aim is the evaluation of fluid-dynamic parameters. Knowledge of density, pressure, temperature, Mach number and so on in the deposition chamber is useful for optimizing the deposition process. More specifically, the influence of: i) mass flow rate ($\dot{m}$), ii) electrical power (E), supplied to the torch, iii) and nozzle geometry (in order to change fluid-dynamic conditions at the inlet of the chamber) have been evaluated. Working gas was just Argon. The computer simulations did not consider the presence of any precursors and therefore of any chemical reactions; thus Argon was considered just like a tracer. Argon was considered not diffusive, but ionization (computed by the Saha formula [12]) was taken into account from an energetic point of view. Figure 2 shows a schematic of the apparatus, modeled in the present computations.

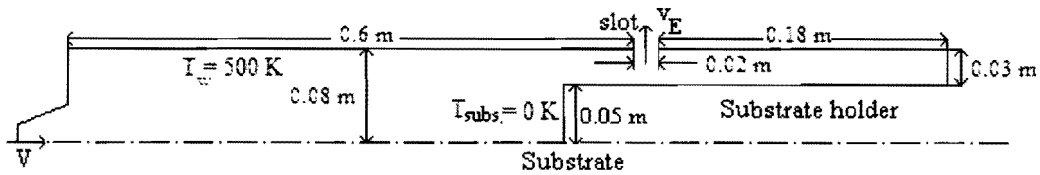

Fig.2 – Schematic of the apparatus

The simulation relies on two codes working in tandem; output from the first one is input to the second one:

1) the first code (or preprocessor) simulates a quasi one-dimensional flow field in a torch and in a conical nozzle. The present simulations are related to the plasma wind tunnel "SPES" at the University of Naples. This plant is made of the torch Perkin-Emler, 9MB-M and a supersonic nozzle. SPES can work with three different conical nozzles,

here labelled A, B, C. The inlet section diameter of all nozzles is the same (0.022 m), the length of the convergent part is 0.046 m for nozzles A and B, 0.025 m for nozzle C. The geometrical characteristics of the divergent parts are:

Nozzle A: throat diameter 0.011 m, exit section diameter 0.022 m (area ratio 4), length 0.061 m,
Nozzle B: throat diameter 0.011 m, exit section diameter 0.05 m (area ratio 20), length 0.1553 m,
Nozzle C: throat diameter 0.008 m, exit section diameter 0.06 m (area ratio 56), length 0.198 m.

Figure 3a,b report the rarefaction parameters Kn_d (λ/d) and $Kn_{L\rho}$ (λ/L_ρ), along the axis of the divergent part of the nozzles. Figure show that the flow field in the nozzle is practically in continuum: $Kn_d<0.1$ and $Kn_{L\rho}<0.1$.

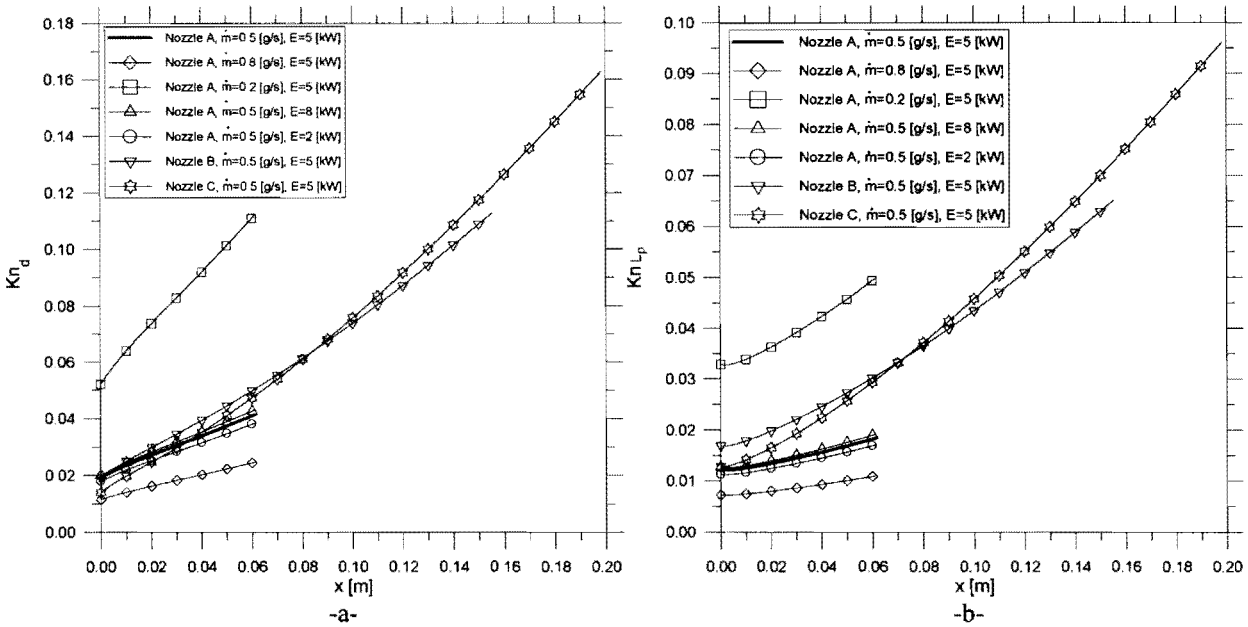

Fig.3 – Profiles of Kn_d (a) and of $Kn_{L\rho}$ (b) along the nozzle axis

2) The second code is DS2V, simulating the flow field in the chamber. Even though the flow field in the nozzle is continuum however, in order to improve the computation by DS2V, all runs started from a point along the nozzle axis at about 90% of the nozzle length. At this station the input data to DS2V (temperature, velocity, number density) are those computed by the preprocessor. Input data to DS2V are reported in table 1 in the columns labeled "Nozzle section", "Chamber", "Exit section". Gas in the chamber has been considered stationary and at typical values of pressure and temperature of 10 N/m^2 and 1500 K [5]. The exit velocity (V_E) has been computed from the mass flow rate, considering pressure and temperature equal to the ones in the chamber:

$$V_E = \frac{\dot{m}}{\rho A_E} \tag{5}$$

where the exit area (A_E) is the area of an annulus slot around the chamber (A_E=0.01 m^2).

Table 1 - Input to DS2V

Test	Nozzle section			Chamber	Exit section
Noz., ṁ [g/s], E[kW]	V [m/s]	T [K]	N [1/m^3]	N [1/m^3]	V_E [m/s]
A, 0.5, 5	2056	2868	1.16×10^{22}	5.06×10^{20}	1482
A, 0.8, 5	2019	2766	1.89×10^{22}	5.25×10^{20}	2288
A, 0.2, 5	2121	3050	4.51×10^{21}	4.76×10^{20}	631
A, 0.5, 8	2088	2957	1.15×10^{22}	4.91×10^{20}	1528
A, 0.5, 2	1998	2709	1.20×10^{22}	5.36×10^{20}	1440
B, 0.5, 5	2786	2359	1.81×10^{21}	6.15×10^{20}	1219
C, 0.5, 5	3221	2456	1.08×10^{21}	5.91×10^{20}	1270

The deposition process is quantified by the sticking factor (γ), defined as the ratio of the number of stuck molecules on the number of impinged molecules. DS2V can simulate the deposition process by considering: i) a diffusive gas-surface interaction model by fixing to 1 the value of α (α is the ratio of the number of molecules reflected diffusively to the total number of impinged molecules), ii) substrate temperature equal to zero; thus the velocity of the re-emitted molecules is, in turn, zero. Consequently molecules remain on the surface, simulating the sticking process. With such an

approach, the sticking factor γ, coincides with α. The present computations considered a fully accommodate model (α=1) therefore a sticking factor equal to 1. The profile of the molecule number flux (N_f) to the substrate, output by DS2V, can be considered as a measure or an indication of the film thickness and of its uniformity.

Data reported in table 1 are "small" shifts from the typical, basic test conditions used by van de Sanden [3, 4, 5]: working gas argon, $\dot{m}$=0.5 g/s, electrical power E=5 kW (second row in table I). As the exit section of nozzle A is pretty similar to the inlet section in the van de Sanden apparatus, the results from these conditions (A, 0.5, 5) will be considered as reference data (in the graphics, these results will be shown by a thick line).

The local Knudsen number Kn_{LV} ($Kn_{LV}=\lambda/L_V$, Fig.4) indicates that only the tests made with small mass flow rate or with nozzles B and C, providing a stronger expansion, overcomes the Navier-Skokes break-down limit ($Kn_{LV}>0.1$).

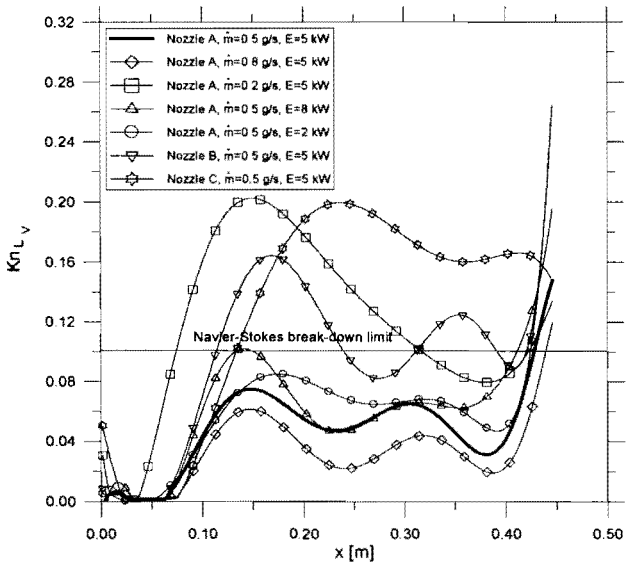

Fig. 4 – Profiles of Kn_{LV} (b) along the chamber axis

Figures 5a,b,c show the two-dimensional maps of the Mach number with the streamline patterns for all tests. These maps verify that the expansion in the nozzle continues in the chamber and is stopped by an abrupt compression due to a shock wave. The supersonic "leaf–blade" area practically does not change extension both with the mass flow rate (a) and with the electrical power (b). It extends along x and reduces along y with the nozzle area ratio (c). As expected the streamlines clearly identify a stagnation zone in the left upper corner and at the end of the chamber after the slot.

As shown in Figs.6a,b, starting from the inlet of the chamber (x=0), the Mach number, and therefore the intensity of the shock wave, increase along the chamber axis. The relative maximum of the Mach number profile: i) increases with the mass flow rate, ii) changes with the nozzle geometry, iii) does not change with the electrical power. Figures 6a,b identify the localization and the extension of the shock wave. The position of the shock wave is defined by abscissa (x_S) where the Mach number attains a relative maximum and its extension or thickness (Δx_S) is defined by the region included between x_S and the point where the Mach number starts to be less than 1. The intensity of the shock wave can be quantified also by the percentage variations of some thermo-fluid-dynamic parameters along the chamber axis.

The profiles of velocity, temperature, pressure and density are reported in Fig.6c thru l. Velocity and temperature decrease practically linearly, downstream the shock wave, while pressure and density remain almost constant. Table 2 reports, for each test, the position, the extension and the maximum Mach number and the percentage variation of these quantities across the shock wave.

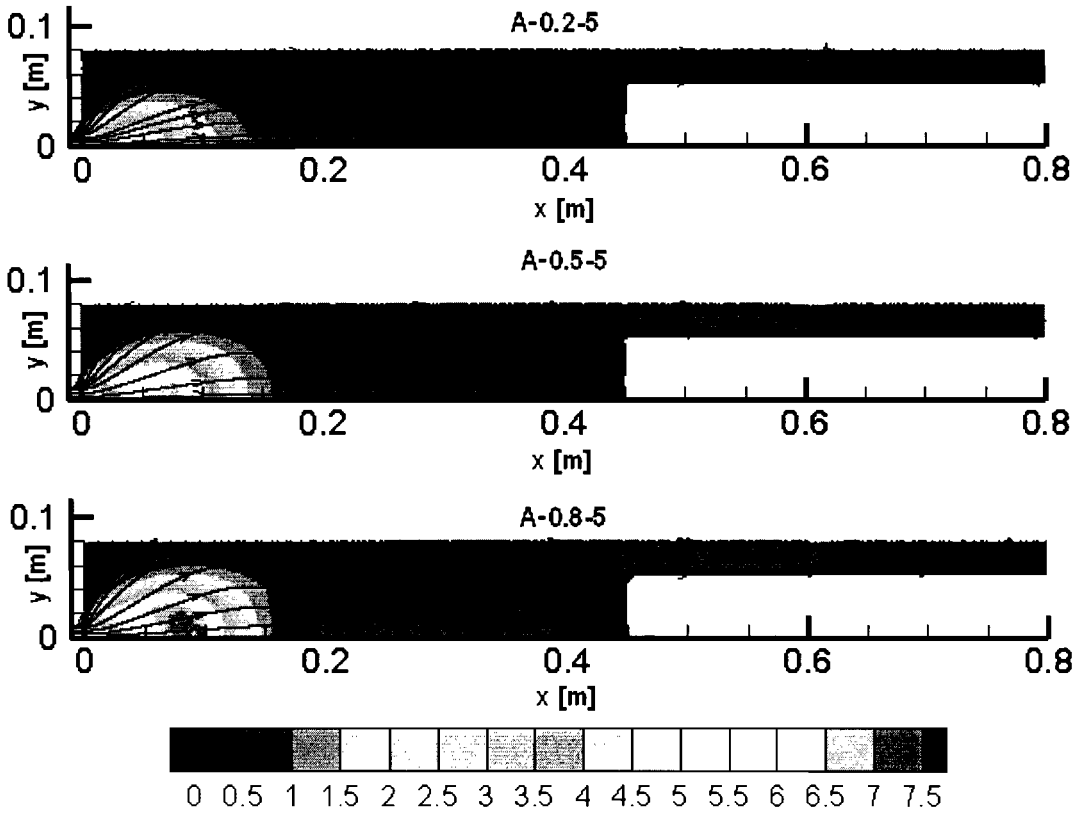
A-0.2-5
A-0.5-5
A-0.8-5
0.1
y [m]
0
0
0.2
0.4
0.6
0.8
x [m]
0 0.5 1 1.5 2 2.5 3 3.5 4 4.5 5 5.5 6 6.5 7 7.5

-a-

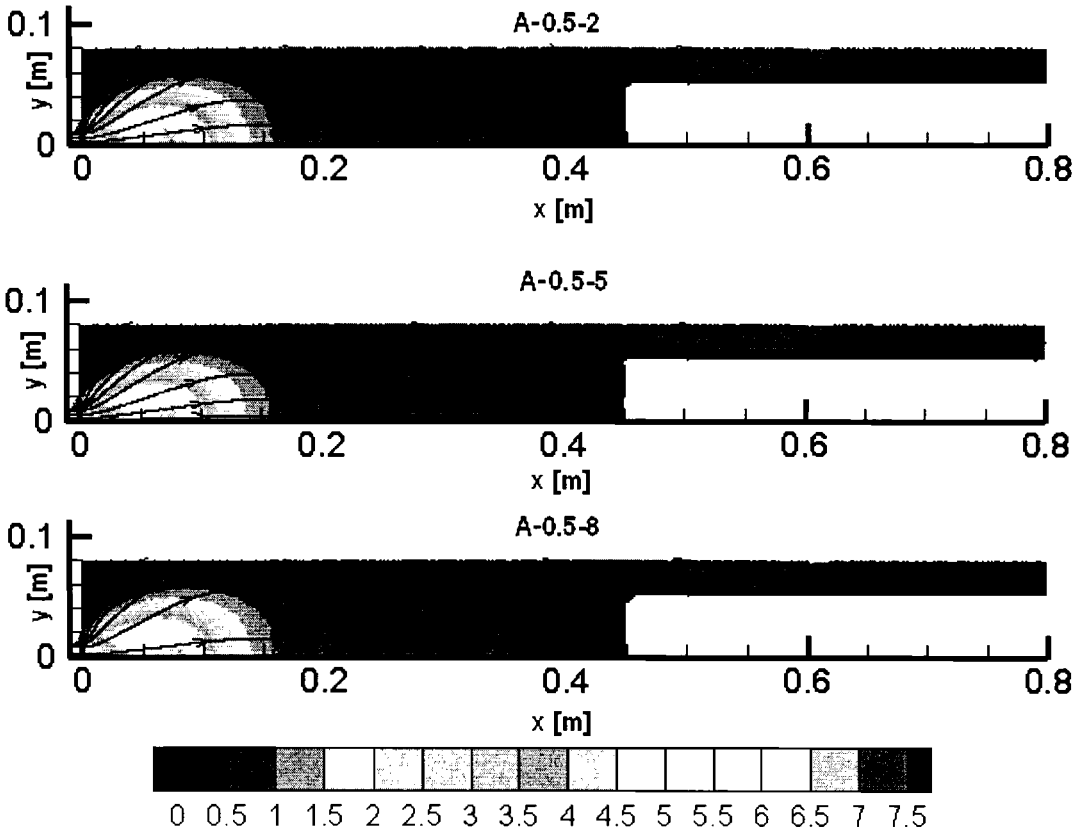
A-0.5-2
A-0.5-5
A-0.5-8
0.1
y [m]
0
0
0.2
0.4
0.6
0.8
x [m]
0 0.5 1 1.5 2 2.5 3 3.5 4 4.5 5 5.5 6 6.5 7 7.5

-b-

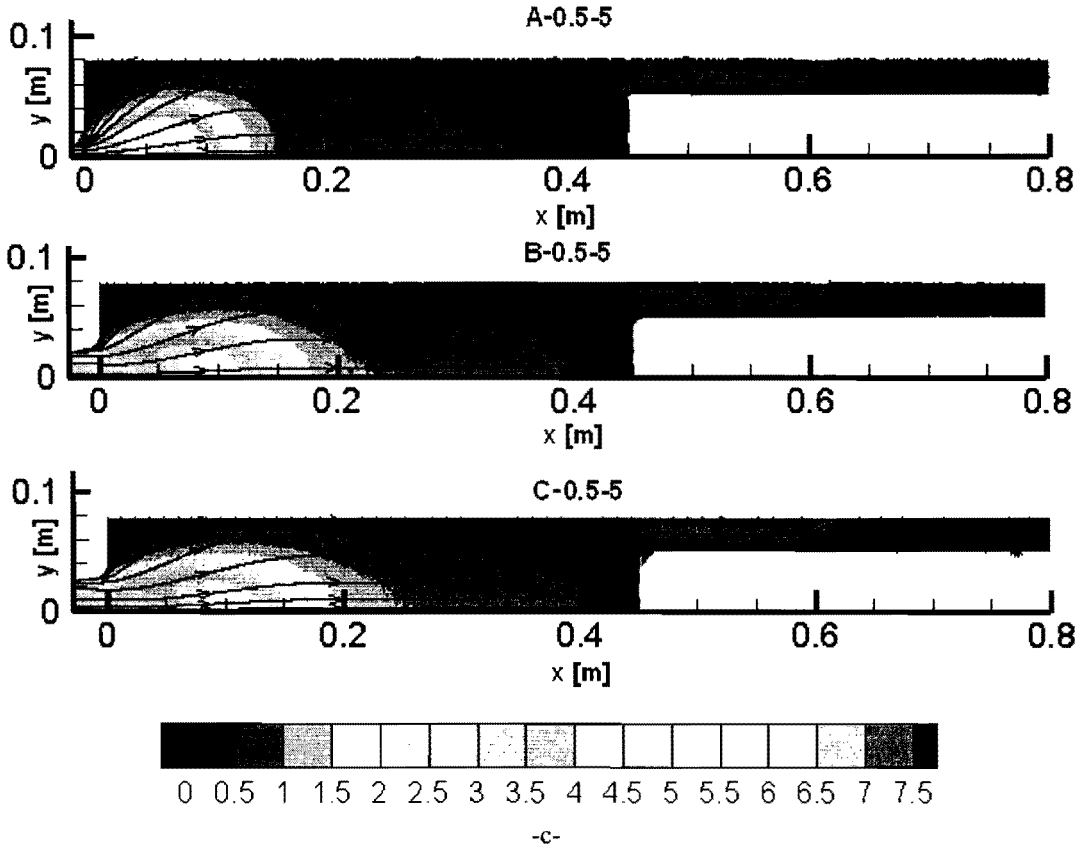

-c-

Fig. 5 – Maps of Mach number and streamline patters in the van de Sanden chamber

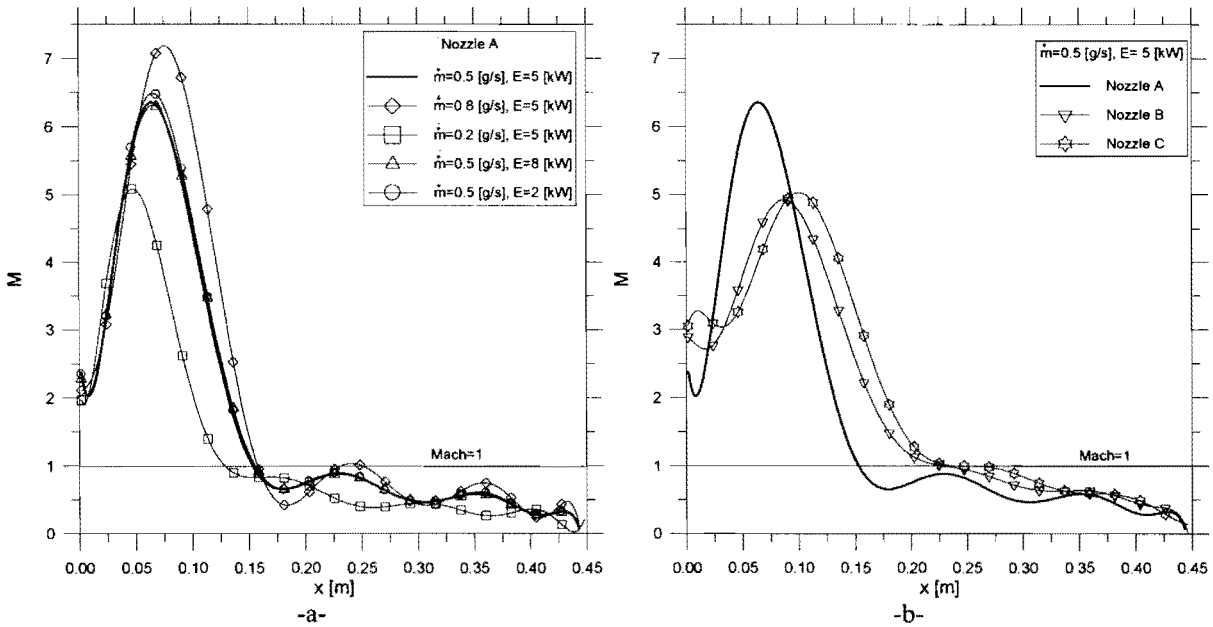

-a- -b-

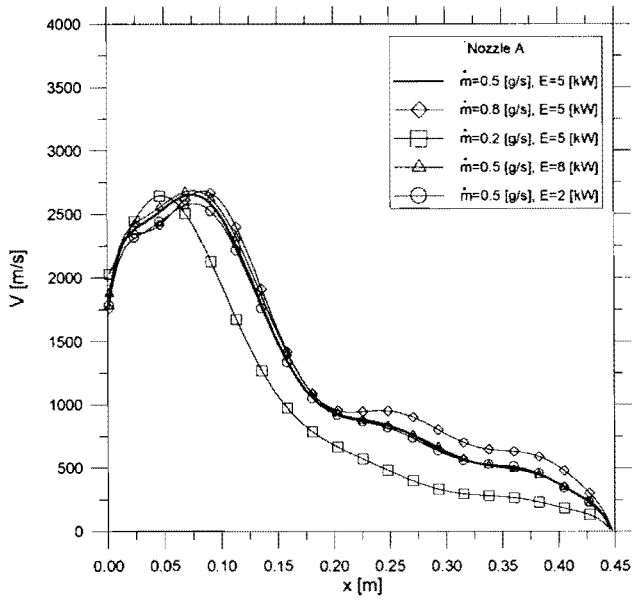
Nozzle A
ṁ=0.5 [g/s], E=5 [kW]
ṁ=0.8 [g/s], E=5 [kW]
ṁ=0.2 [g/s], E=5 [kW]
ṁ=0.5 [g/s], E=8 [kW]
ṁ=0.5 [g/s], E=2 [kW]
V [m/s]
x [m]

-c-

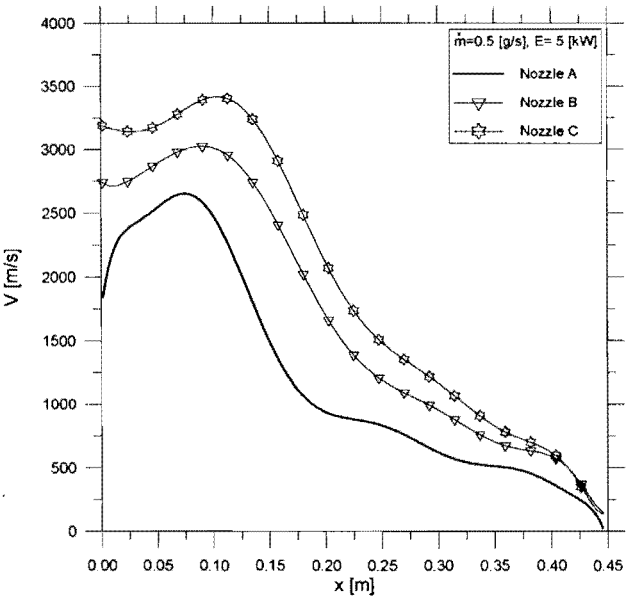
ṁ=0.5 [g/s], E= 5 [kW]
Nozzle A
Nozzle B
Nozzle C
V [m/s]
x [m]

-d-

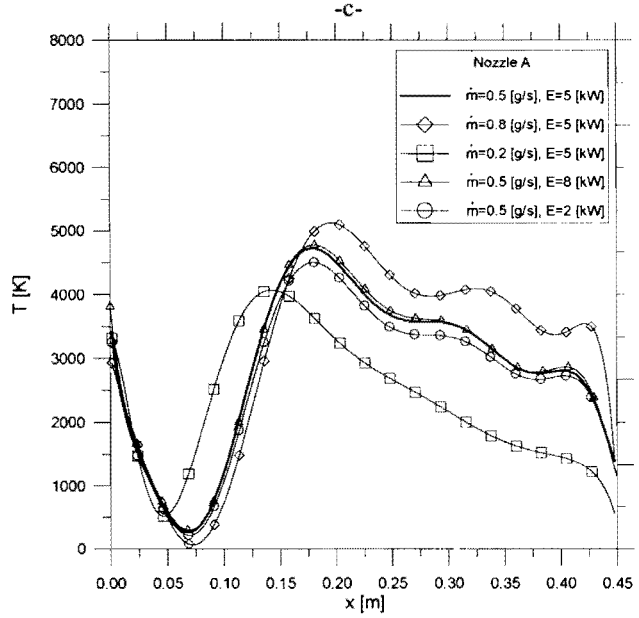
Nozzle A
ṁ=0.5 [g/s], E=5 [kW]
ṁ=0.8 [g/s], E=5 [kW]
ṁ=0.2 [g/s], E=5 [kW]
ṁ=0.5 [g/s], E=8 [kW]
ṁ=0.5 [g/s], E=2 [kW]
T [K]
x [m]

-e-

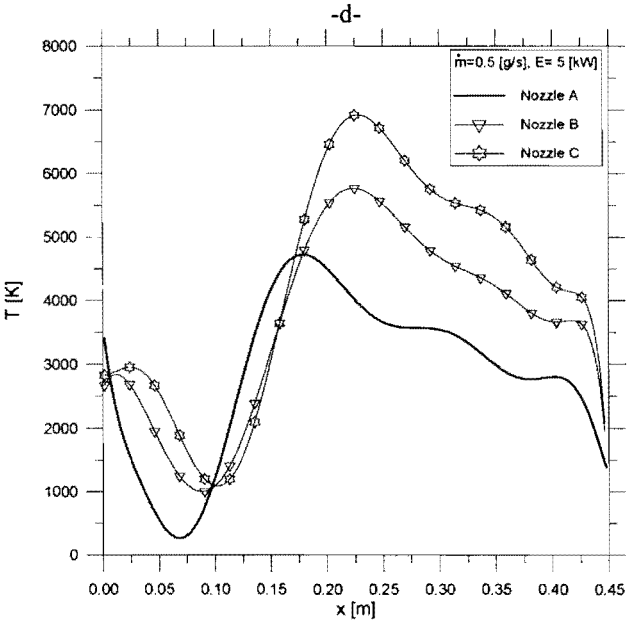
ṁ=0.5 [g/s], E= 5 [kW]
Nozzle A
Nozzle B
Nozzle C
T [K]
x [m]

-f-

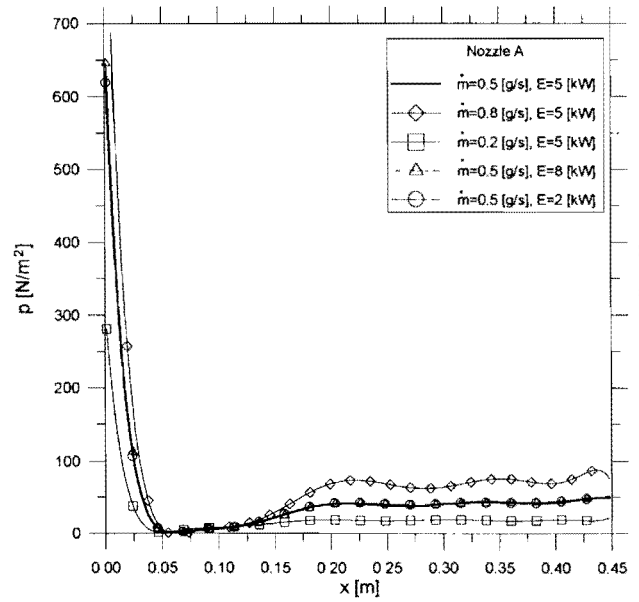
Nozzle A
ṁ=0.5 [g/s], E=5 [kW]
ṁ=0.8 [g/s], E=5 [kW]
ṁ=0.2 [g/s], E=5 [kW]
ṁ=0.5 [g/s], E=8 [kW]
ṁ=0.5 [g/s], E=2 [kW]
p [N/m²]
x [m]

-g-

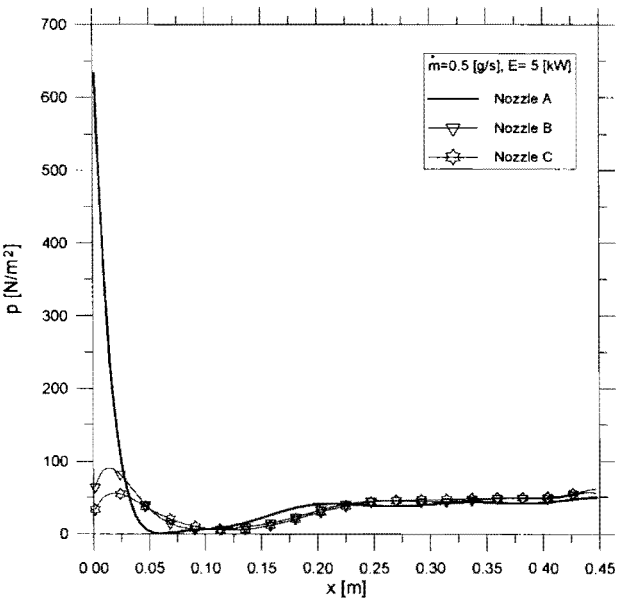
ṁ=0.5 [g/s], E= 5 [kW]
Nozzle A
Nozzle B
Nozzle C
p [N/m²]
x [m]

-h-

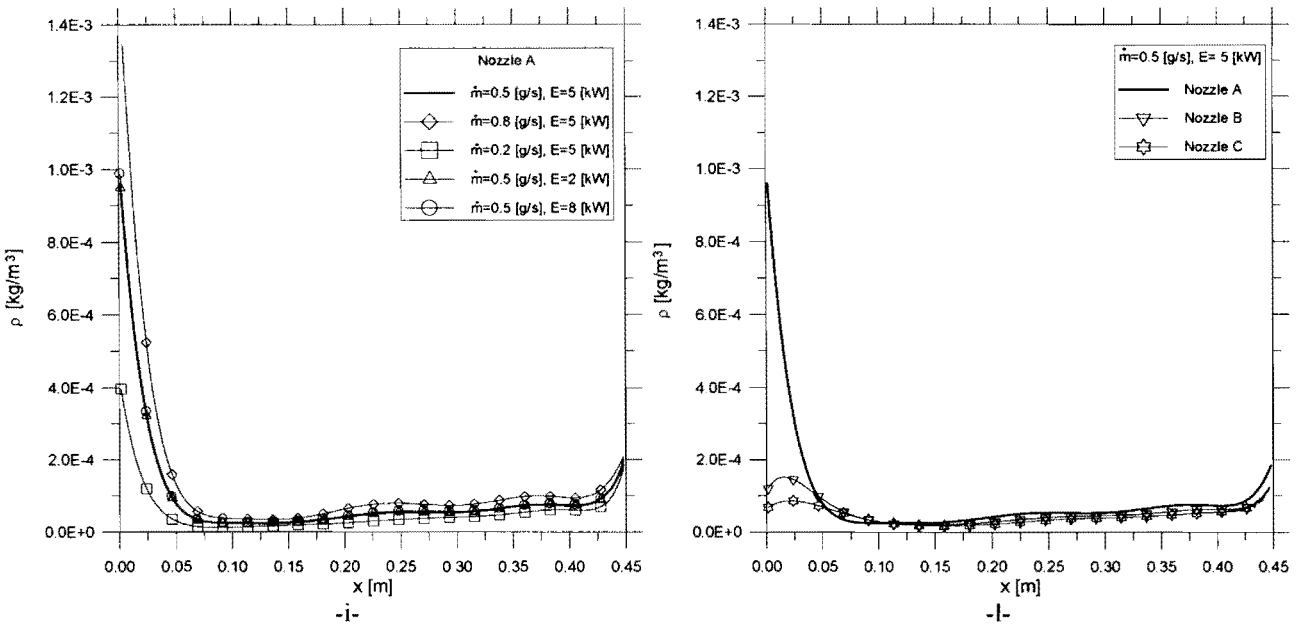

Fig.6 - Profiles of Mach number (a,b), velocity (c,d), temperature (e,f), pressure (g,h), density (i,l) along the chamber axis in terms of mass flow rate, electrical power and nozzle

Table 2 – Position and extension of the shock wave and percentage variation of some parameters

Noz., ṁ [g/s],E[kW]	x_s [m]	M_{max}	Δx_s [m]	ΔM/M%	ΔV/V%	ΔT/T%	Δp/p%	Δρ/ρ%
A, 0.5, 2	0.075	6.49	0.082	-87	-51	1263	1094	-12
A, 0.5, 5	0.080	6.40	0.079	-86	-52	1086	904	-15
A, 0.5, 8	0.080	6.35	0.079	-87	-55	1193	1101	-7
A, 0.2, 5	0.056	5.10	0.091	-84	-60	487	367	-20
A, 0.8, 5	0.097	7.20	0.057	-87	-45	1591	1478	-7
B, 0.5, 5	0.092	4.90	0.133	-81	-53	489	482	-1
C, 0.5, 5	0.120	5.00	0.118	-82	-53	548	807	40

Figures 7a,b show the profiles of number flux ($N_f \times 10^{-24}$ $m^{-2}s^{-1}$) of molecules impinged onto the substrate. The lower is the mass flow rate, the smaller is the number flux and therefore the thickness of the film. Consequently the thickness distribution is more uniform. Electrical power does not influence the thickness and its uniformity (Fig.7a). It looks from Fig.7b that the larger is the nozzle exit section, the smaller is uniformity. A measure of the thickness and of its uniformity is provided by the average of N_f and by the standard deviation, respectively, both reported in Table 3.

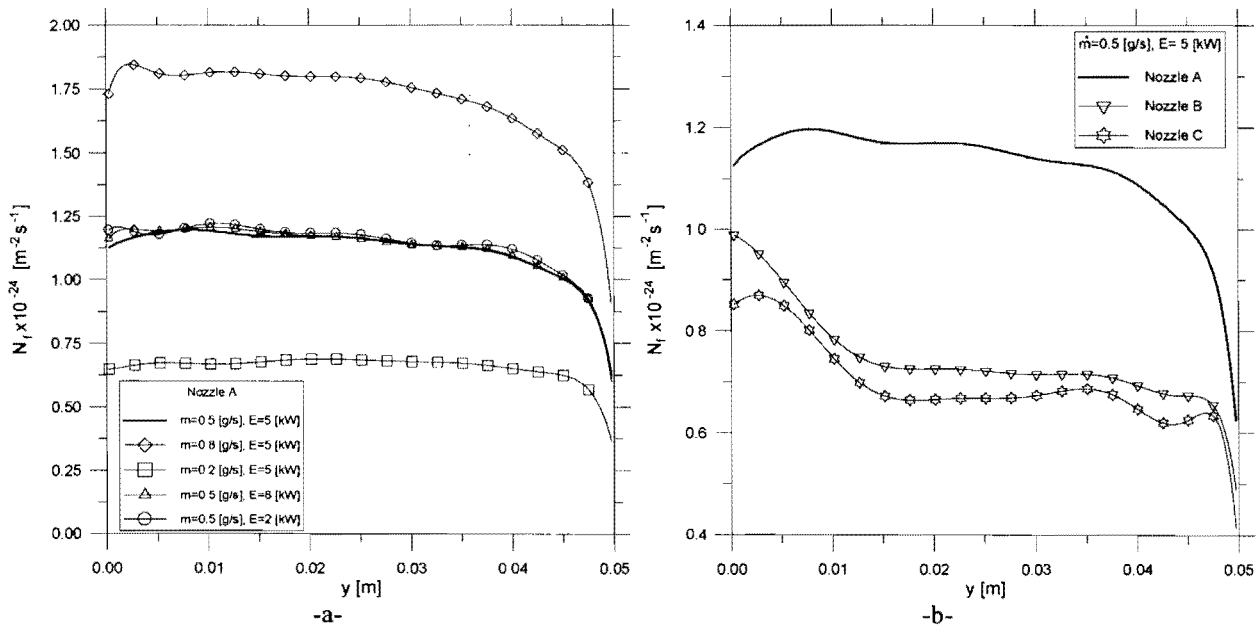

Fig.7 – Flux number profile along the substrate in terms of mass flow rate, electrical power (a) and nozzle (b)

Table 3 – Film deposition parameters

Noz., $\dot{m}$ [g/s],E[kW]	Average [$m^{-2}s^{-1}$]	Standard deviation [$m^{-2}s^{-1}$]
A, 0.5, 2	1.14	0.11
A, 0.5, 5	1.12	0.10
A, 0.5, 8	1.13	0.11
A, 0.2, 5	0.66	0.05
A, 0.8, 5	1.71	0.17
B, 0.5, 5	0.74	0.10
C, 0.5, 5	0.69	0.09

MICRO-CHANNEL

The Micro-Electro-Mechanical Systems (MEMS) are becoming increasingly important, due to their characteristics of tiny size, small mass and rapid response time. Currently MEMSs are used in many areas such as: micro-motors, robotics, automotive engineering, computer technology, avionics, medicine, and so on.

The micro-channels are essential elements of MEMS therefore, in order to enhance their design and performance, a deep understanding of their fluidics and an evaluation of heat transfer and pressure distribution are required. Recent investigations [6, 7, 8] have shown that the flow behaviour in MEMS is different from that in a macro-system. In fact, the mean free path of molecules is of the same order of magnitude as a typical geometrical dimension of the micro-channel, as per height (H); the Knudsen number is of the order of 1 ($Kn_H=\lambda/H\cong O(1)$) or higher and the flow field could be better described by method based on molecular approach, compared with those based on classical CFD.

The aim of the present tests is completing the very meaningful analysis by Le [6]. More specifically, the present computations are carried out in order to evaluate the effects of rarefaction on two important mechanical parameters like load loss (Y) and impulse (I) as well as on Mach number. By definition, Y and I read:

$$Y = k\frac{(V_i - V)^2}{2g} \tag{6.a}$$

$$I = p + \rho V^2 \tag{6.b}$$

where g is the gravitational acceleration ($g=9.81$ m/s^2), k is a constant depending on the channel geometry (in the present calculations $k=1$) and V_i is the velocity at the inlet section of the channel. The interest to these parameters is justified by the fact that the task of a micro-channel is transferring pressure information from the measurement point to the transducer. On the other hand, due to the small dimensions of a micro-channel, the Reynolds number is rather low, therefore the viscous force dominates over the inertial force and its influence could be strong enough to alter the measured pressure.

Tests were carried out at the same conditions like the ones by Le and Hassan [6]. The flow rarefaction level was changed only by changing the molecule number density. The original test conditions used by Le and Hassan are here reported:

2-D plane micro-channel
Length, L=6 μm,
Height, H=1.2 μm,
Working gas: nitrogen,
T_w=323 K,
V=1500 m/s,
T=300 K,
M=4.2
$\rho=8.1\times10^{-1}$ Kg/m^3
$N=1.8\times10^{25}$ 1/m^3

The results, obtained by this input, have to be considered as reference results for those obtained by the following values of number density: $N=5.0\times10^{24}$, 1.0×10^{25}, 3.5×10^{25} and 7.3×10^{25} 1/m^3. Figure 8 shows the profiles of Kn_H along the micro-channel center-line. The profiles verify that the flow field in the channel can be considered in continuum low density regime, therefore suitable to be processed by a DSMC code.

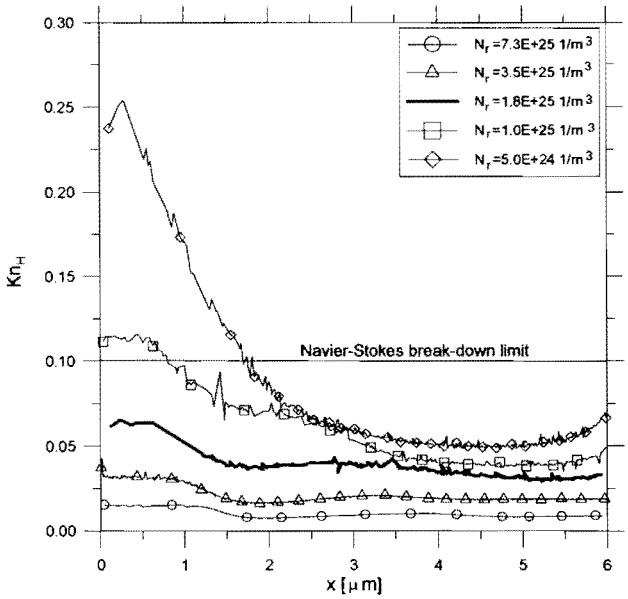

Fig. 8 – Profiles of Kn_H along the micro-channel center-line

Figures 9a,b, 10a,b and 11a,b show the profiles of load loss, impulse and Mach number along the center-line (a) and along the exit section (b) of the channel at the above mentioned Knudsen numbers. The influence of rarefaction is pretty strong; for example, along the center-line of the channel, the average value of Y changes from 373 to 4.8×10^4 m, of I changes from 1.3×10^7 to 4.0×10^5 N/m^2 and of M changes from 3.5 to 0.9 in the interval of Kn_H from 0.015 to 0.22. Figures 9b, 10b and 11b show that increasing rarefaction improves the uniformity of profiles. In fact, the standard deviation of the load loss ranges from 2.4×10^4 to 6.3×10^3 m, of the impulse ranges from 4.1×10^6 to 5.7×10^4 N/m^2 and of the Mach number from 0.81 to 0.14. Figure 11a verifies that the effects of rarefaction are particularly strong on the Mach number. In fact, even starting from a supersonic value, at Kn_H=0.22 the Mach number decreases up to a subsonic values (at x=2.02 μm) and then increases once again to a supersonic value (at x=5.64 μm). This is due to a decrease of velocity and to an increase of temperature (see Fig.12a,b) produced by a strong viscous effect.

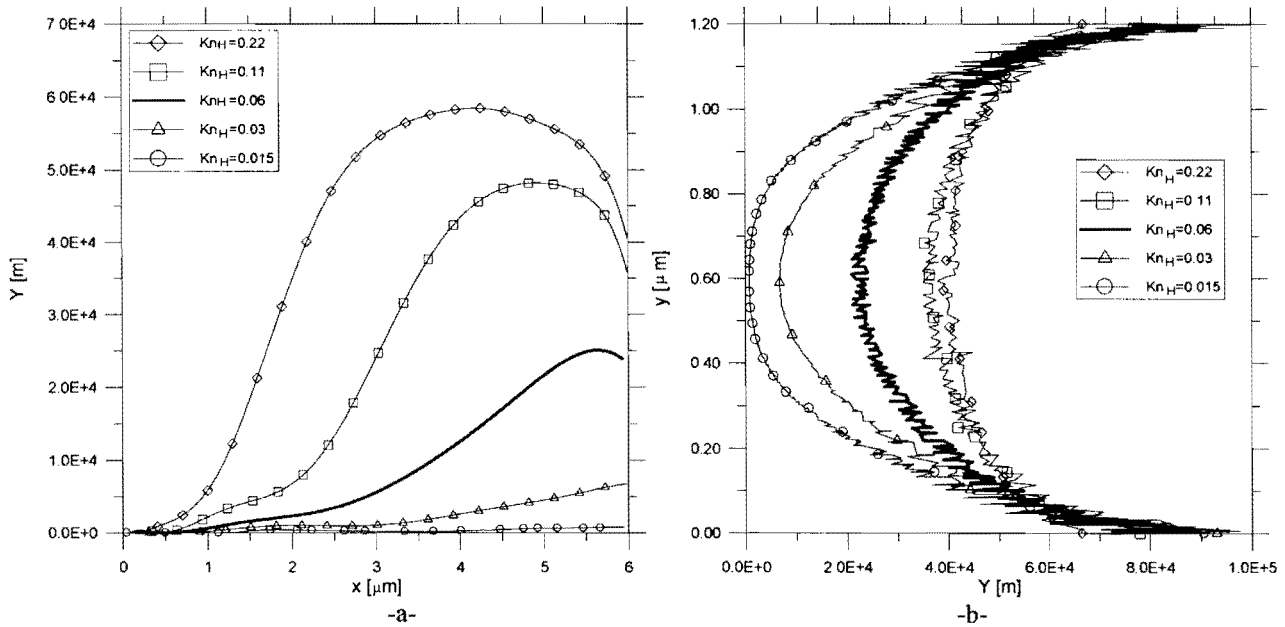

Fig.9 – Profiles of load loss along the center-line (a) and along the exit section (b) of the channel at different Knudsen numbers

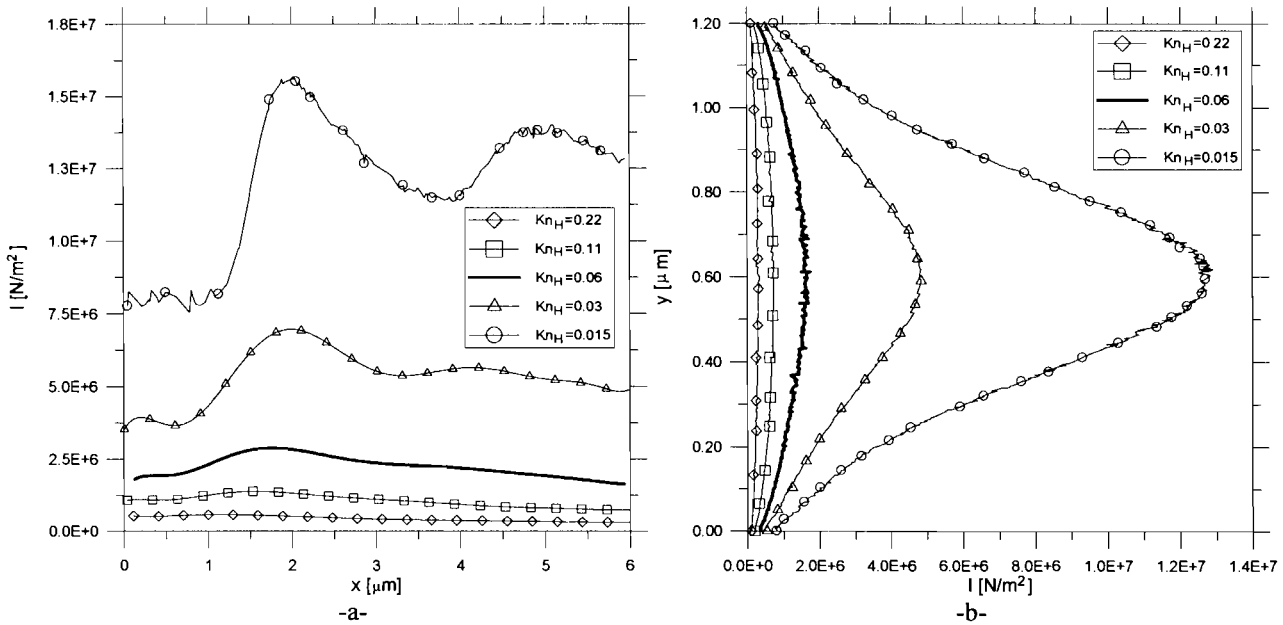

Fig.10 – Profiles of impulse along the center-line (a) and along the exit section (b) of the channel at different Knudsen numbers

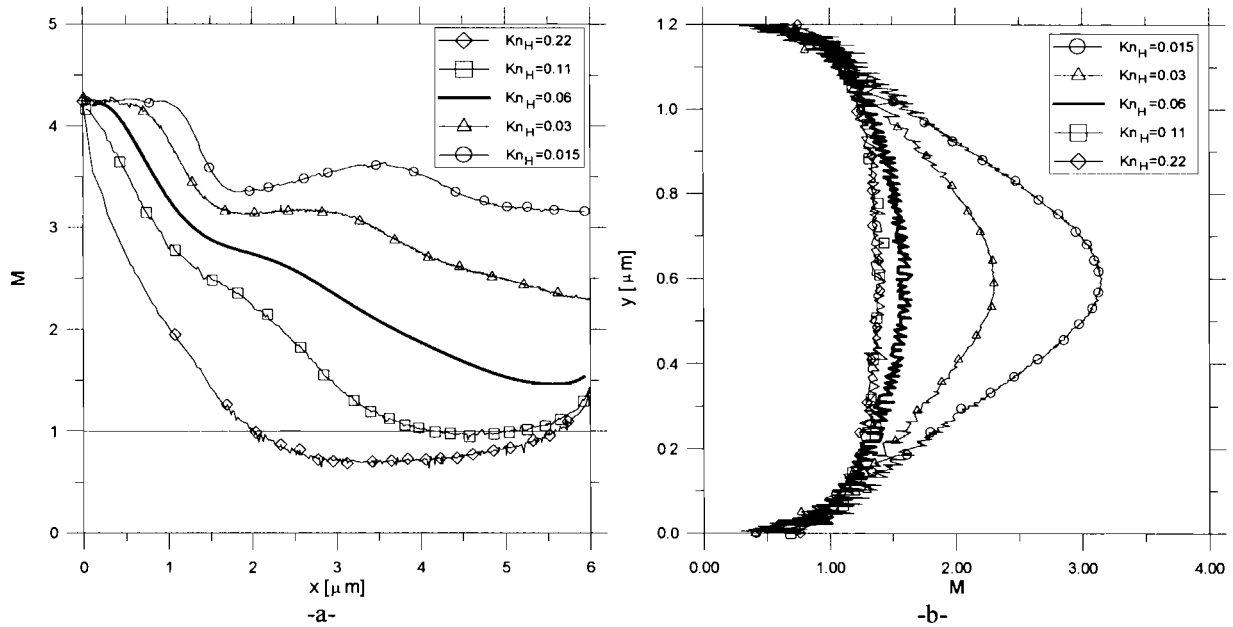

Fig.11 – Profiles of Mach number along the center-line (a) and along the exit section (b) of the channel at different Knudsen numbers

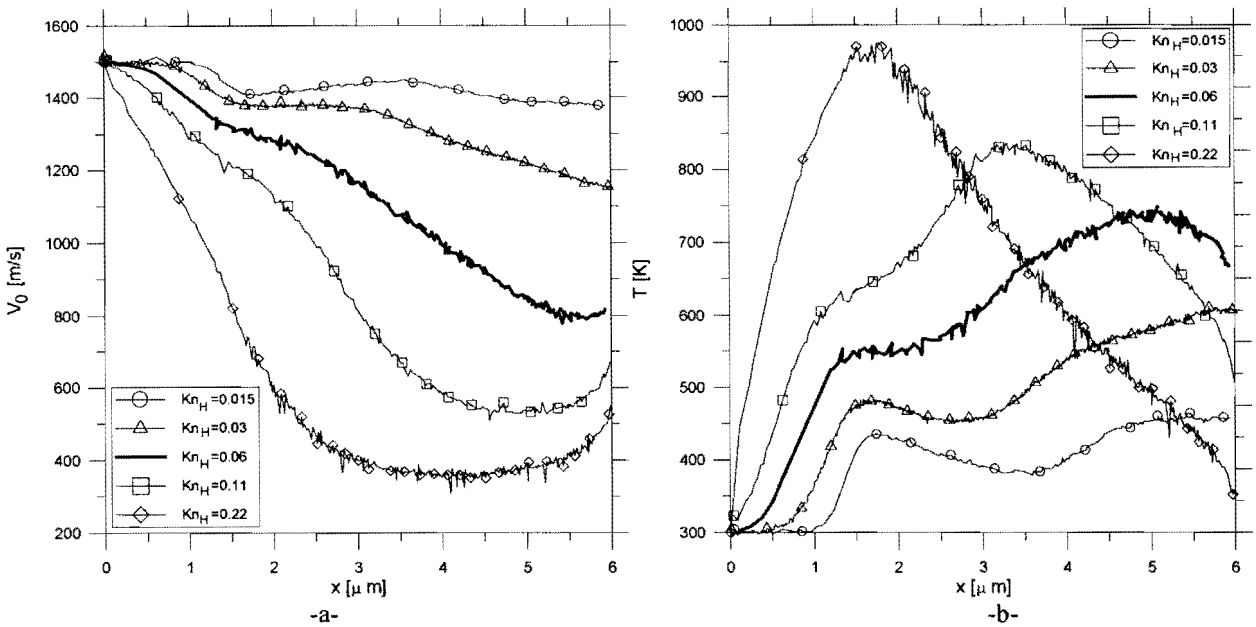

Fig. 12 – Profiles of velocity (a) and of temperature (b) along the channel center-line

TRANSPORT COEFFICIENTS

As well known, viscosity μ [Kg/m/s] is computed, as a function of temperature, by the well known Chapman-Enskog theory [13, 14]:

$$\mu = \frac{2.6693 \times 10^{-6} \sqrt{mT}}{d^2 \Omega_\mu} \tag{7}$$

where: m is the molecular mass, Ω_μ is the collision integral for viscosity. Viscosity of a mixture is evaluated, by the Wilke rule, from the coefficients of each species and from the gas composition or molar fractions of each species (α_i, i=1,…,n):

$$\mu = \sum_{i=1}^{n} \frac{\alpha_i \mu_i}{\sum_{j=1}^{n} \alpha_j \Phi_{i,j}} \tag{8}$$

where:

$$\Phi_{i,j} = \frac{1}{\sqrt{8}} \left(1 + \frac{m_i}{m_j}\right)^{-1/2} \left[1 + \left(\frac{\mu_i}{\mu_j}\right)^{1/2} \left(\frac{m_j}{m_i}\right)^{1/4}\right]^2 \tag{9}$$

A correct evaluation of μ is important also for an evaluation of thermal conductivity k [W/m/K]. In fact for:

- monatomic gases $k = \frac{15}{4} R\mu$ (10)
- poly-atomic gases $k = \left(c_p + \frac{5}{4} R\right)\mu$ (11)

R and c_p are the constant and the specific heat at constant pressure of gas, respectively.

Even though the Chapman-Enskog formula and the Wilke rule are widely accepted and used, their calculation could be complicate and time consuming. In engineering/industrial applications, it could be practical and convenient evaluating the transport coefficients in a more easy and immediate way. The Sutherland law and the exponential law [13, 14] are able to evaluate the viscosity as a function of temperature by knowledge of viscosity (μ_{ref}) at a given temperature (T_{ref}), usually T_{ref}=273 K:

- Sutherland law: $\mu = \mu_{ref}\left(\frac{T_{ref}+C}{T+C}\right)\left(\frac{T}{T_{ref}}\right)^{1.5}$ (12)

- exponential law: $\mu = \mu_{ref}\left(\frac{T}{T_{ref}}\right)^{\omega}$ (13)

where C is a constant and ω is the temperature exponent, both depending on gas. The values of the temperature exponent are reported in the open literature for a number of gases [1], while the values of C are less diffuse.

This section describes and verifies a method, based on DSMC computations, for a direct evaluation of viscosity for a mixture of gases, without computing separately the viscosity of each species and therefore without using the Wilke rule. The method computes the viscosity by the Newton phenomenological equation:

$$\mu = \frac{\tau_0}{(\partial u/\partial y)_0} \tag{14}$$

where τ_0 and $(\partial u/\partial y)_0$ are the tangential shear stress and the velocity tangential gradient at the wall, respectively. The present evaluation of viscosity relies on the solution of the flow field on a flat plate. As the flow field is isobaric, the velocity profile at the wall is linear. This makes easier the numerical approximation of the gradient of the velocity tangential component at the wall; thus Eq.14 reads:

$$\mu \cong \frac{\tau_0}{(u_{y^*} - u_0)/y^*} \tag{15}$$

where: u_{y^*} is velocity at $y=y^*$ and u_0 is the slip velocity at the wall.

A number of tests have been made and the accuracy of the method has been evaluated by means of the comparison with the Chapman-Enskog-Wilke results and, where possible, with the Sutherland (12) and the exponential laws (13). The simulations considered:

1 m length flat wall,
u_∞=300 m/s,
$N_\infty=1.4\times10^{20}$ m^{-3},
$T_\infty=T_w$= 273, 385, 500, 625, 750, 875, 1000 K,
Pure gases:
Argon, Helium, Nitrogen, Oxygen.
Mixture of gases:
Argon-Helium, mole fractions: 0.2, 0.8,
Oxygen-Nitrogen, mole fractions: 0.21, 0.79,
Argon-Oxygen-Nitrogen, mole fractions: 0.4, 0.3, 0.3,
atomic Oxygen-atomic Nitrogen-Helium, mole fractions: 0.3, 0.5, 0.2,
Nitrogen-Oxygen-atomic Oxygen-Helium, mole fractions: 0.6, 0.2, 0.1, 0.1,
Nitrogen-atomic Nitrogen-Oxygen-atomic Oxygen-Argon, mole fractions: 0.3, 0.1, 0.3, 0.1, 0.2.

Gases were considered "real"; thus for bi-atomic molecules, rotation, vibration, dissociation and exchange reactions can be activated. For all tests, τ_0 and velocity gradient were evaluated at about x=0.5 m and y^*=0.028 m. Temperature exponent ω (see Eq.13) is finally evaluated by fitting a number of viscosity coefficients, as a function of temperature.

Figure 13 reports some profiles of the Tsien parameter (Kn_δ), computed at x=0.5 m, as functions of the free stream temperature. The minimum and the maximum values are met by N_2 and by the mixture O-N-He, respectively. In the same figure the profiles for two intermediate cases (Ar, and the mixture N_2-O_2-O-He) are reported for completeness. According to the above mentioned criterion, at the calculation point, the flow field is in continuum low density regime, therefore suitable for a DSMC application.

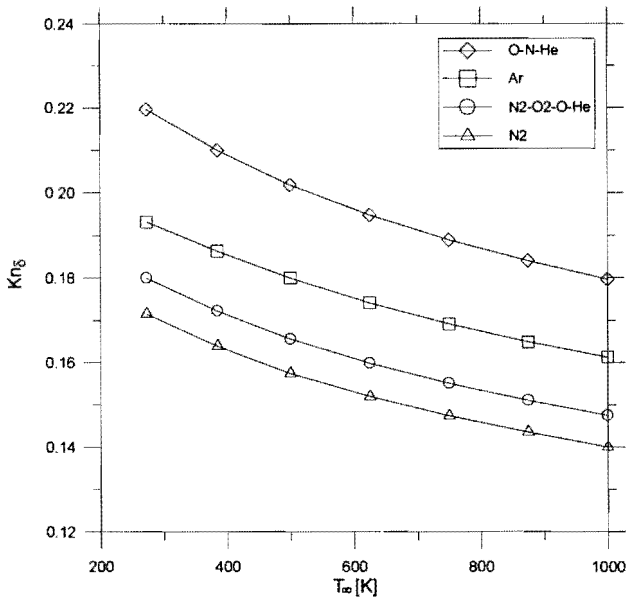

Fig. 13 – Profiles of the local Knudsen number, based on the boundary layer thickness evaluated at x=0.5 m

Figures 14a thru l show the viscosity profiles as functions of temperature. Figures 14a thru c show the viscosity profiles for Ar, O_2, and N_2. Figures 14d thru f show the viscosity profiles for the above mentioned mixtures of these gases. These figures verify that the comparison of the present results with those from the Chapman-Enskog theory, from the Sutherland and the exponential law is pretty good. More specifically, for Ar, O_2, N_2, and some mixture of these gases the comparison is excellent up to a temperature of 600-700 K. A small mismatch has to be pointed out at higher temperatures. Unfortunately, it has to be also noticed that the present method fails for He (Fig.14g). This is probably due to a poor computation of the tangential shear stress that, in turn, is due to the light weight of helium. For this reason, evaluating a power law interpolation was not possible. The bad behaviour of helium influences also the correctness of the results of a mixture (Fig.14h, l). As expected, the higher is the mole fraction of He the stronger is the mismatch with the Chapman-Enskog results.

The DSMC exponents (ω_{DSMC}), for gases Ar, O_2, N_2 and their mixtures, are reported in table 4 where the coefficients ω, used in the exponential laws, are taken from literature [1]. Table 5 reports the minimum, maximum and average values of the percentage variation of the DSMC viscosity with respect to the Chapman-Enskog-Wilke results.

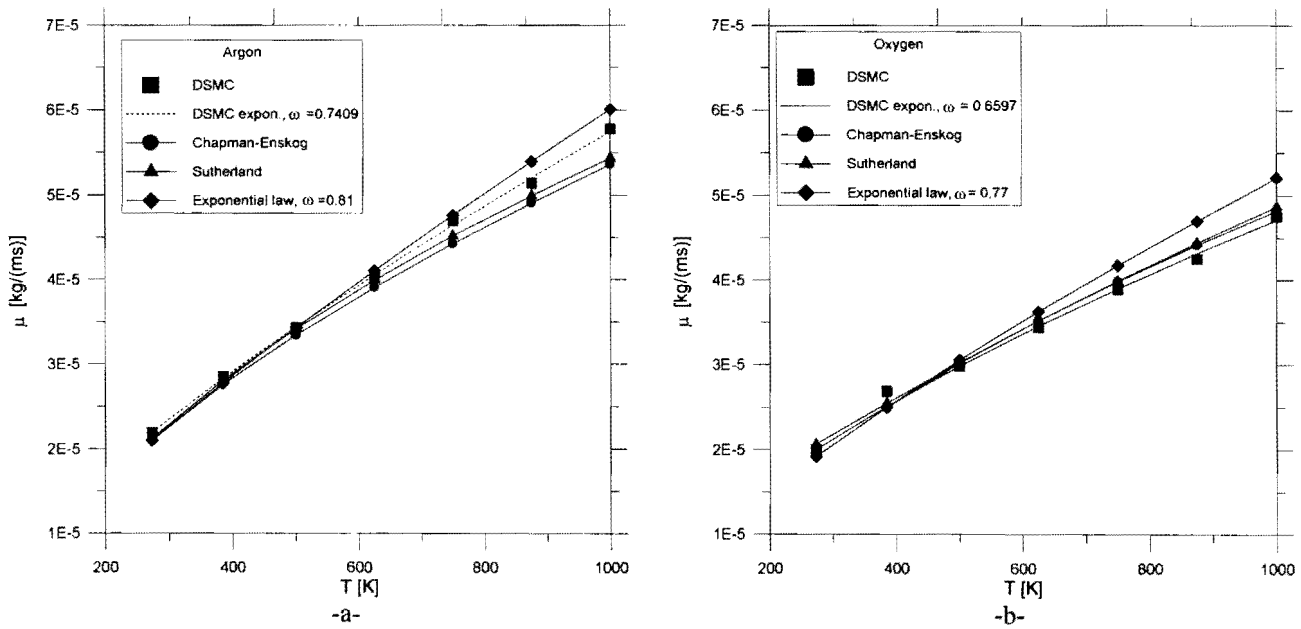

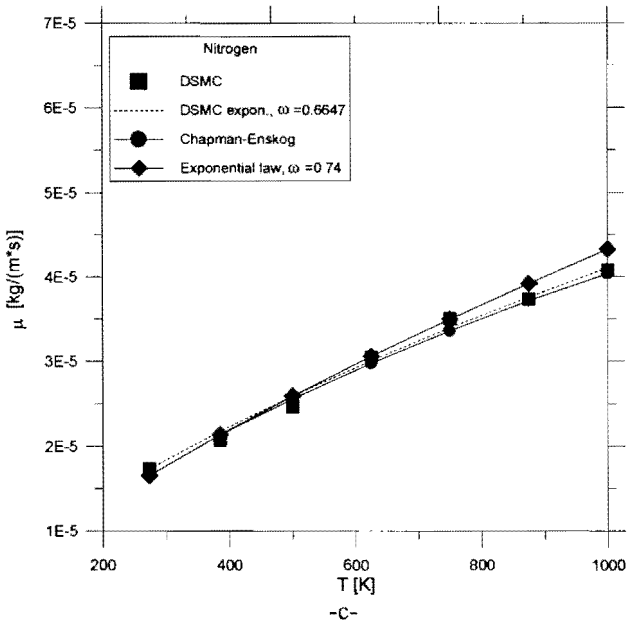
Nitrogen
DSMC
DSMC expon., ω =0.6647
Chapman-Enskog
Exponential law, ω =0.74
μ [kg/(m*s)]
T [K]

-c-

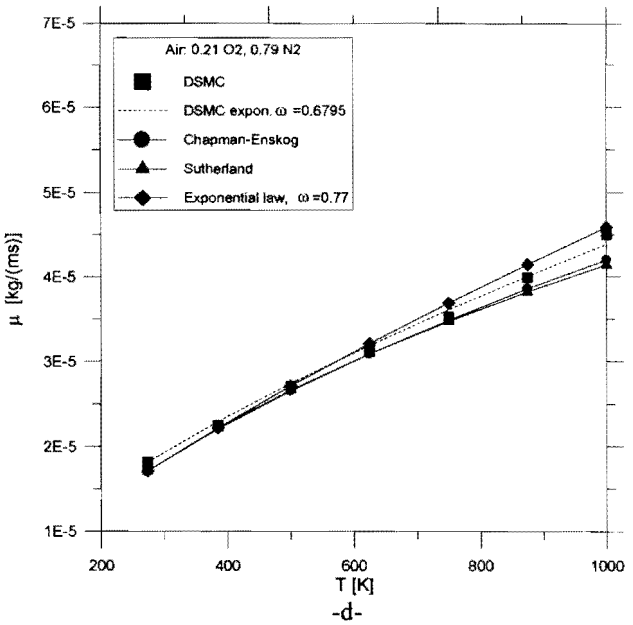
Air: 0.21 O2, 0.79 N2
DSMC
DSMC expon. ω =0.6795
Chapman-Enskog
Sutherland
Exponential law, ω =0.77
μ [kg/(ms)]
T [K]

-d-

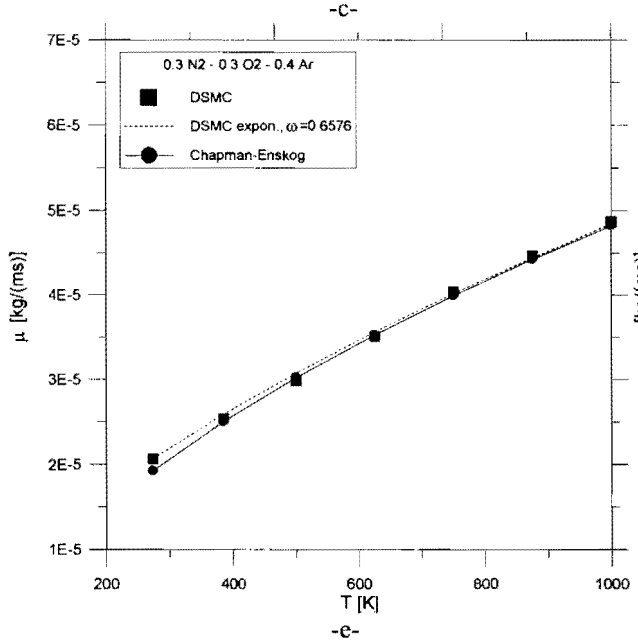
0.3 N2 - 0.3 O2 - 0.4 Ar
DSMC
DSMC expon., ω=0.6576
Chapman-Enskog
μ [kg/(ms)]
T [K]

-e-

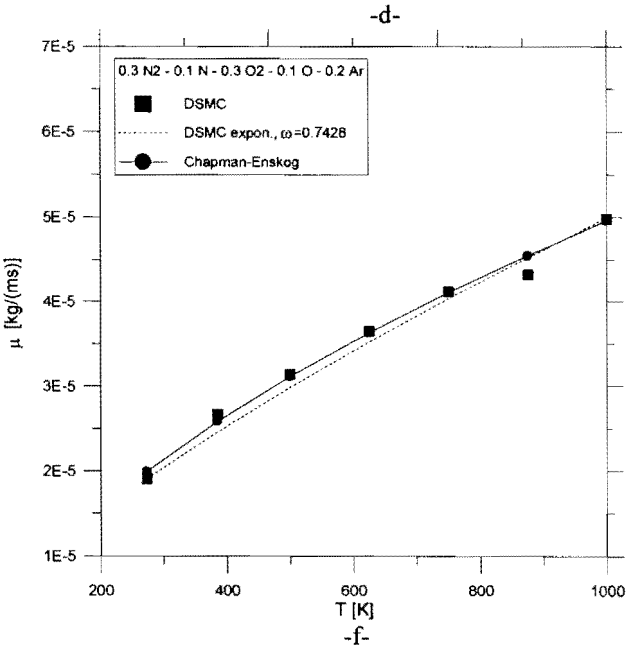
0.3 N2 - 0.1 N - 0.3 O2 - 0.1 O - 0.2 Ar
DSMC
DSMC expon., ω=0.7428
Chapman-Enskog
μ [kg/(ms)]
T [K]

-f-

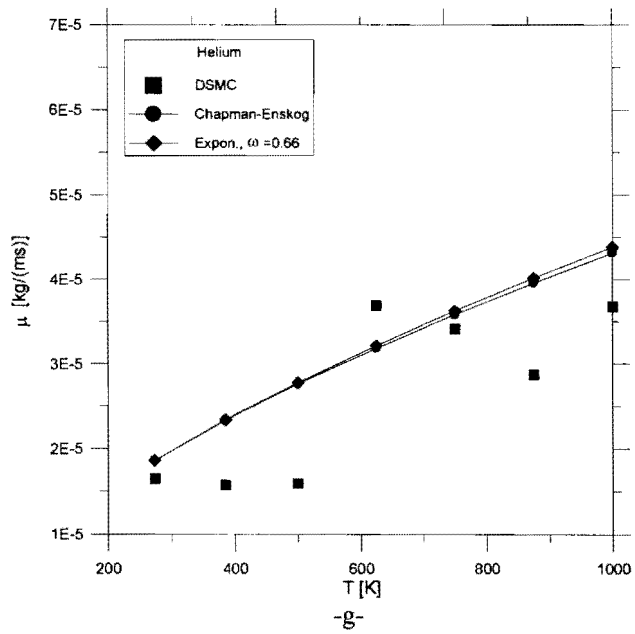
Helium
DSMC
Chapman-Enskog
Expon., ω =0.66
μ [kg/(ms)]
T [K]

-g-

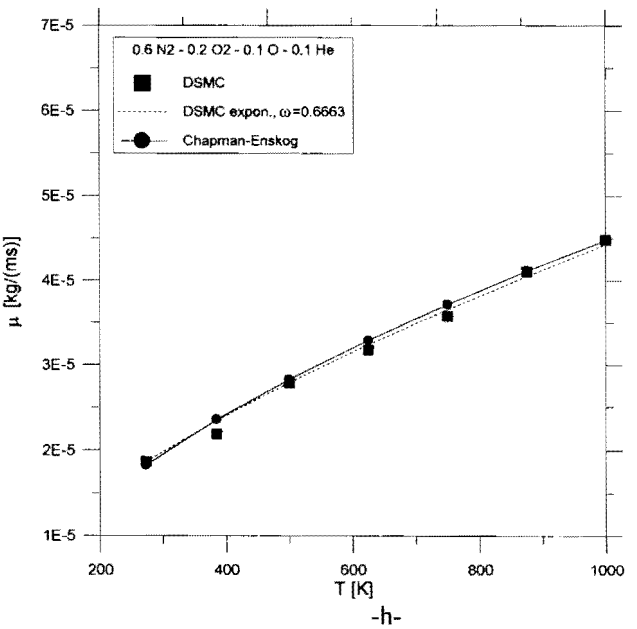
0.6 N2 - 0.2 O2 - 0.1 O - 0.1 He
DSMC
DSMC expon., ω=0.6663
Chapman-Enskog
μ [kg/(ms)]
T [K]

-h-

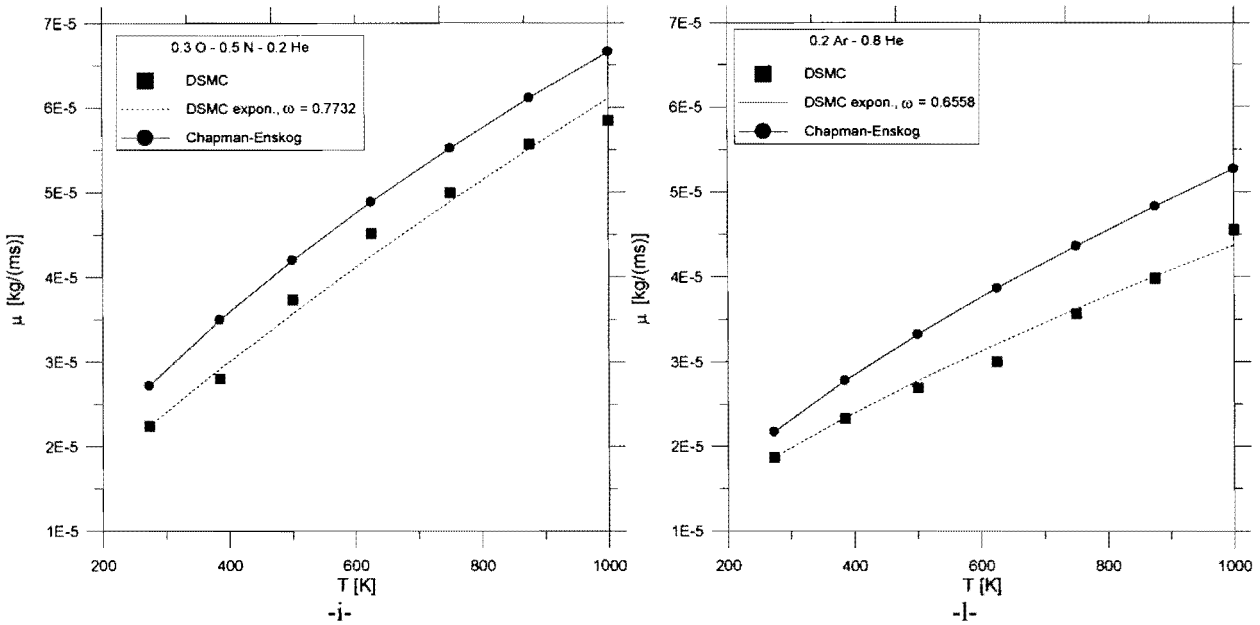

Fig.14 – Viscosity profiles for argon (a), oxygen (b), nitrogen (c) and air (d), mixture of argon, oxygen, nitrogen (e), mixture of nitrogen, atomic nitrogen, oxygen, atomic oxygen, argon (f), helium (g), mixture of oxygen, nitrogen, atomic oxygen, helium (h), mixture of atomic oxygen, atomic nitrogen and helium (i), mixture of argon, helium (l), as functions of temperature

Table 4 – Temperature exponential coefficients

	Ar	O_2	N_2	Air	Ar-O_2-N_2	N_2-N-O_2-O-Ar
ω_{DSMC}	0.7409	0.6597	0.6647	0.6795	0.6576	0.7428
ω [1]	0.81	0.77	0.74	0.77		

Table 5 – Percentage variation of viscosity

	Ar	O_2	N_2	Air	A_r-O_2-N_2	N_2-N-O_2-O-Ar
Min.	2.81	-2.3	1.05	3.27	0.47	-4.81
Max.	7.16	4.4	4.64	6.14	7.48	0.72
Average	4.63	-0.68	1.88	4.04	2.19	-2.50

CONCLUSIONS AND FURTHER DEVELOPMENTS

Starting from the works of a number of researchers, published in open literature, three different possible industrial applications of the DSMC method have been revised and improved. The most updated version (Ver 4.5) of the "sophisticated" DS2V code has been used to simulate the flow field:

1. in a deposition chamber at different values of the mass flow rate, of the electrical power provided to the torch and using three different supersonic nozzles. A preliminary method for the estimation of the film thickness distribution on the substrate is also proposed. A sensitivity analysis of: electrical power to the torch and of different fluid-dynamic conditions, linked to nozzle geometry, has been carried out. This analysis verified that the electrical power does not influence the thickness and its uniformity. On the opposite it verified that the larger is the exit section of the nozzle, the smaller is the thichness uniformity.
2. In a micro-channel for the evaluation of important parameters like the load loss and impulse. The influence of rarefaction on these parameters has been quantified.
3. On a flat plate for the evaluation of the exponent of the law of viscosity for a mixture of gases.

Further developments of this research activity will be related just to the deposition chamber. Precursor C_2H_2 will be considered and the related chemical reactions will be implemented both in the pre-processor and in DS2V.

REFERENCES

1) Bird G. A., *Molecular Gas Dynamics and Direct Simulation Monte Carlo*, Clarendon Press Oxford Science, 1998
2) Shen, C., *Rarefied Gas Dynamic: Fundamentals, Simulations and Micro Flows*, Springer-Verlag, Berlin, 2005
3) van de Sanden M. C. M., Severens R. J., Gielen J. W. A. M., Paffen R. M. J. and Schram D. C., *Deposition of a-Si:H and a-C:H Using an Expanding Thermal Arc Plasma*, Plasma Sources Sci. Technol., May 1996, pp. 268-274
4) van de Sanden M. C. M., Regt J.M. and Schram D. C., *The Behaviour of Heavy Particles in the Expanding Plasma Jet in Argon*, Plasma Sources Sci. Technol., March 1994, pp. 501-510
5) Selezneva S,E., Boulos M.I., van de Sanden M. C. M., Engeln R., Schram D.C., *Stationary Supersonic Plasma Expansion: Continuum Fluid Mechanics Versus Direct Simulation Monte Carlo Method*, J. Phys. D: Appl. Phys., 35, 2002, pp 1362-1372
6) Le, M., Hassan, I., *Simulation of Heat Transfer in High Speed Microflows*, Applied Thermal Engineering, 26, 2006, pp 2035-204
7) Arkilic, E., Schmidt, M.A., Breuer, K., *Gaseous Slip Flow in Long Microchannels*, Journal of Microelectromechanical Systems, Vol.6, (2), 1997, pp 167-178
8) Ho C., Tai, Y., *Micro-Electro-Mechanical Systems (MEMS) and Fluid Flows*, Annual Review Fluid Mechanics, Vol.30, 1998, pp 579-612
9) Bird, G.A., *The DS2V Program User's Guide, (Version 4.3) included in the program*, G.A.B. Consulting Pty Ltd, Sydney (Aus.), June 2006
10) Bird, G.A., *Sophisticated Versus Simple DSMC*, Proceedings of the 25th International Symposium on Rarefied Gas Dynamics, Saint-Petersburg (Russia), July 2006
11) Bird, G.A., *Sophisticated DSMC*, Notes from a Short Course held at the DSMC07 Conference, Santa Fe (USA), Sep. 30- Oct. 3, 2007
12) Cobine, J. D., *Gaseous conductors theory and engineering applications,* Dover Publication Inc., New York, 1958.
13) Bird, R.B., Stewart, W.E., Lightfoot, E.N., *Fenomeni di Trasporto* (in Italian), Ambrosiana, Milano, 1970
14) Anderson, J.D., *Hypersonic and High Temperature Gas-Dynamics*, McGrw-Hill, New York,1989